Accepted Manuscript

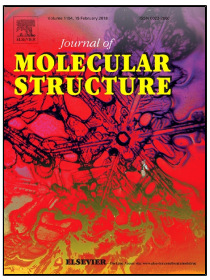

Rhodamine B Removal on A-rGO/Cobalt Oxide Nanoparticles Composite by Adsorption from Contaminated Water

Salam.H.Alwan Altaa, Hassan.A.Habeeb Alshamsi, Layth.S.Jasim Al-Hayder

PII:	S0022-2860(17)31615-0
DOI:	10.1016/j.molstruc.2017.11.127
Reference:	MOLSTR 24614
To appear in:	*Journal of Molecular Structure*
Received Date:	21 October 2017
Revised Date:	28 November 2017
Accepted Date:	29 November 2017

Please cite this article as: Salam.H.Alwan Altaa, Hassan.A.Habeeb Alshamsi, Layth.S.Jasim Al-Hayder, Rhodamine B Removal on A-rGO/Cobalt Oxide Nanoparticles Composite by Adsorption from Contaminated Water, *Journal of Molecular Structure* (2017), doi: 10.1016/j.molstruc.2017.11.127

Highlights

1. A-rGO/Co_3O_4 was prepared, used as an adsorbent to remove Rh.B from wastewater.

2. The adsorption kinetics was rapid with 8h to reach the equilibrium.

3. The q_e for Rh.B is 102.9 mg g^{-1}, an excellent surface for the removal of dye.

4. It was found that the adsorption reaction an endothermic and spontaneous.

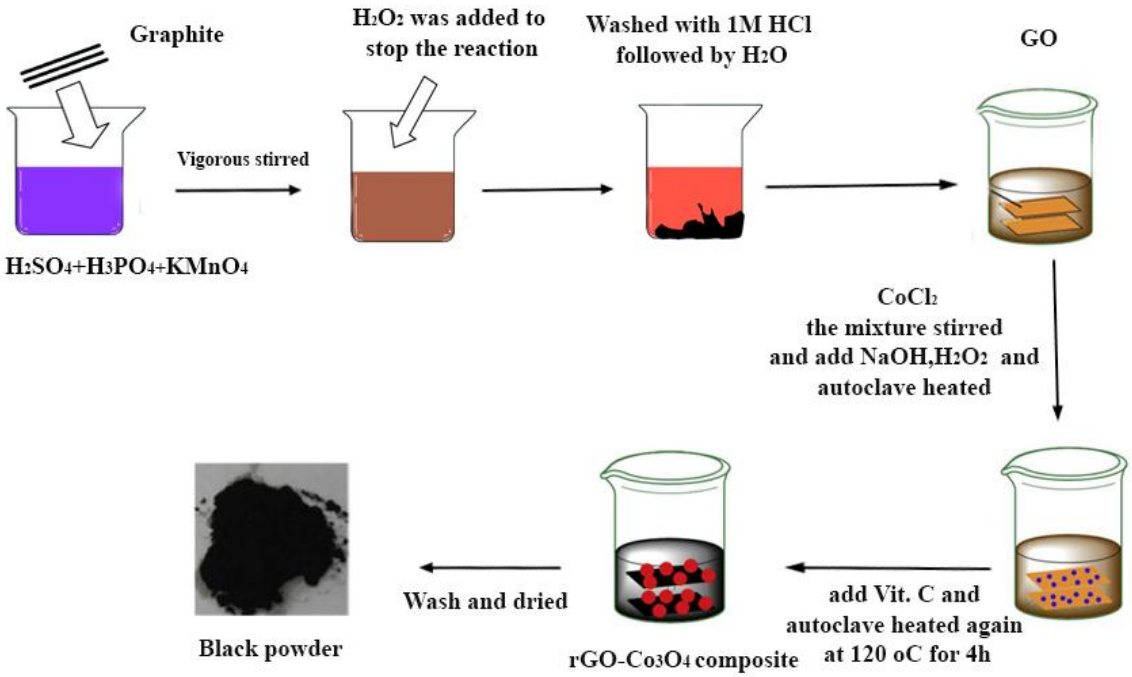
Graphite
H2O2 was added to stop the reaction
Washed with 1M HCl followed by H2O
GO
Vigorous stirred
H2SO4+H3PO4+KMnO4
CoCl2
the mixture stirred and add NaOH,H2O2 and autoclave heated
add Vit. C and autoclave heated again at 120 oC for 4h
rGO-Co3O4 composite
Wash and dried
Black powder

Rhodamine B Removal on A-rGO/Cobalt Oxide Nanoparticles Composite by Adsorption from Contaminated Water

Salam H. Alwan Altaa*[1], Hassan A. Habeeb Alshamsi[1], Layth S. Jasim Al-Hayder[1]
[1]Department of Chemistry, College of Education, University of Al-Qadisiyah, Diwaniya 1753, Iraq
*Corresponding author: Tel.: +9647808163781
E-mail addresses: salamhussein354@gmail.com

Abstract

Cobalt oxide nanoparticles@rGO composite is prepared by using graphene oxide (GO) as a supporting substance. GO is first treated with ascorbic acid to form rGO. Finally, cobalt oxide nanoparticles reaction with rGO sheets and using as the adsorbent to removal Rh.B dye from wastewater. The morphology and chemical structure of prepared samples were characterized by FTIR, X-ray spectroscopy, SEM-EDX, TEM, AFM and TGA. The adsorption of Rh.B dye on the A-rGO/Co_3O_4 composite was accomplished under different conditions that are equilibrium time, pH solution, ionic strength, and temperature. The adsorption isotherms of Rh.B dye on the A-rGO/Co_3O_4 composite could be illustrated well by the Langmuir, Freundlich and Tempkin model. The thermodynamic factors (ΔH^o, ΔS^o, and ΔG^o) estimated from the temperature-dependent isotherms revealed that the adsorption reaction of Rh.B dye on the A-rGO/Co_3O_4 composite was an endothermic and spontaneous process.

Keywords: Rhodamine B, A-rGO/Co_3O_4, Nanoparticles, Adsorption isotherms, Thermodynamic factors

1. Introduction

Rhodamine B cationic dye is commonly used in paper printing, paint, textile dyes and leather industries. So remove that dye from the sewage to protect water, environment and public health. The dye toxicity of affects not only the plants but also the effect of a carcinogen in humans and animals because they possess the bioaccumulation characteristic[1]. There are many methods of treatment dyes including filtration, chemical coagulation, biological oxidation, active sludge, solvent extraction, photodegradation, flocculation and adsorption have been used for the elimination of dyes from polluted wastewaters[2, 3]. Adsorption technique has attracted researchers attention in recent years due to its high efficiency, low cost and ease of work[4]. Different materials, for example, dirt minerals, oxides, zeolites and carbon materials have been utilized as adsorbents. In any case, there are still a few issues that hat limit from users, for example, adsorption ratio is not sufficiently high; the adsorbent is hard to separate. Accordingly, searching for new adsorbents to solve these problems are of great interest[5]. These days, the investigation of nanomaterial-based composites for water treatment is still in the beginning times. To design effective technique for the manufacture of nanomaterials is yet a test[6]. Recently, graphene oxide (GO) attracted the attention of many researchers attributed to the large theoretical specific surface area (~2630 $m^2\ g^{-1}$) and has been demonstrated as a successful sorbent for the expulsion of

dyes and organic contamination. Consequently, it can be proficiently exfoliated and functionalized obtain on homogeneous suspensions in both water and organic solvents. Giving greater probability to a preparation of graphene-based materials. The presence of oxygen functional groups and aromatic sp^2 areas permit GO to take an interest in forming bonds with other materials [7-9]. To obtain the productivity of the adsorbent materials, graphene papers ought to be decoration with nanoparticles to give a composite shape that has awesome properties for instance high conductivity, high particular surface zone, quick electronic exchanges, astounding mechanical adaptability and great chemical stability[10, 11].

In this study, rGO was used in a template form of Co_3O_4 nanoparticle that inhibits agglomeration of metal oxide and effectively reduces the size. It is worth mentioning that GO was reduced by using ascorbic acid. The A-rGO/Co_3O_4 nanocomposite was prepared and used to remove Rhodamine B dye from the contaminated water with studying all the adsorption conditions. Finally, characterization prepared materials using various techniques identify the morphology of the A-rGO/Co_3O_4 nanocomposite and size particles.

2. Experimental Part

2-1.Materials Used

Ascorbic acid, L-tryptophan, H_2SO_4, H_3PO_4, Ethanol were obtained from B.D.H Company and used directly without primary purification. H_2O_2, NaOH were supplied from Scharlau. $KMnO_4$, $NaNO_3$ and Rh.B were supplied from Merck. All solutions were prepared using deionized water.

2-2.Characterization

Fourier Transform Infrared Spectroscopy (FT-IR) analysis was accomplished by a Nicolet Nexus 670 FT-IR instrument with KBr tablets as sample holders in the 400–4000cm^{-1} region. X-ray diffraction (XRD) analysis using a D/Max 2550 V diffractometer with Cu Kα radiation (λ = 1.54056 Å) (Rigaku, Tokyo, Japan), and the XRD data were 60 collected at a scanning rate of 0.03°s^{-1} for 2θ in a range from 5° to 80°. The morphology of prepared materials was noted by scanning electron microscopy (JEOL, JSM-6701F, Japan) operated at an acceleration voltage of 8.0 kV. Transmission electron microscopy (TEM) observations were performed using Jeol 2100 TEM under an accelerating voltage of 200 kV. Atomic force microscopy (AFM) was performed utilizing a Park Systems XE-70 Atomic Force Microscope in non-contact style. Thermogravimetry (TGA) measurement was conducted by the Perkin-Elmer Diamond high-temperature thermal analyzer with 5-20mg samples and a heating rate of 10 ^oC min^{-1} from 50 to 600 ^oC in an Ar.

2-3. Preparation of Co_3O_4 Nanoparticles and A-rGO/Co_3O_4 Composites

The graphene oxide (GO) was obtained from pristine graphite powder using a modified Hummers method[12]. The synthesis of A-rGO/Co_3O_4 nanocomposite was performed by hydrothermal method. Where 0.1g graphene oxide is placed in a flask

containing 200 ml of deionized distilled water and inserted into the ultrasonication bath for 1h. The other step is to add an aqueous solution 10 ml of $CoCl_2$ (1.4 g $CoCl_2$. $6H_2O$) to the solution above and stirred for 2h to complete their reaction. Then add drops of 10 ml sodium hydroxide and stirred the solution for 1h. In addition, add 30%, 1.5 ml H_2O_2 to the mixture above and insert the total solution into Teflon-lined autoclave and heat to 100°C for 4h. After ending the period, 0.25 g L-(+)-ascorbic acid is added as a reducing agent, introduce mixture into the Teflon-lined autoclave and heated to 120 °C for 4h. The final powder is assembled using a centrifugal method, washing with deionized distilled water several times, then drying the product and the calcination at 150°C for 5 h to obtain rGO/Co_3O_4 nanocomposite[13]. While Co_3O_4 nanoparticles were prepared using the solvothermal process. Mixing 0.6 g $Co(NO_3)_2.9H_2O$ and 3.3 g SDBS were dissolved in 40ml absolute ethanol and leave the mixture in the ultrasonication bath for a 0.5h dark green solution is obtained. Then insert the solution into the Teflon-lined autoclave and heat it to 180 °C for 4h. The powder is dried in vacuum at 90 °C for 6h. finally, calcination of product at 400 °C for 4h to obtain black crystalline cobalt oxide (Co_3O_4) [14, 15]. While rGO was obtained from GO by reduction with Ascorbic acid[16].

2-4. Rh.B Adsorption Experiments

Solutions of dye (10ml) of known concentrations 5-200 ppm were added to stoppered flasks containing 0.01 g of A-rGO/Co_3O_4 nanocomposite. The flasks were shaken in a thermostatically controlled water bath at a speed of 150 rpm until equilibrium is attained 8h. These times are sufficient for the adsorption process to reach equilibrium in each case. After the equilibrium time elapsed, the suspensions were a centrifuged at 3000 rpm for 10min. Spectrophotometrically by using a UV-Visible spectrophotometer. Equilibrium concentrations were obtained by comparing the experimental data with the calibration curve. The quantity of dye adsorbed was calculated according to the following equation[17].

$$q_e = \frac{V_{sol.}(C_o - C_e)}{m} \quad \text{..... (1)}$$

$$\text{Removal\%} = \frac{(C_o - C_e)}{Co} * 100 \quad \text{..... (2)}$$

Where q_e is the sorption capacity (mg/g), m is the weight of adsorbent (g), C_o is the initial concentration (mg/L), C_e is the equilibrium concentration (mg/L) and V is the volume of solution (L). The effect of different factors was also studied such as the weight of A-rGO/Co_3O_4 nanocomposite, pH, temperature, and ionic intensity on adsorption of dye and calculating the amount of material absorbed per agent.

3-Results and Discussion

3-1.Characterization

Figure (1) shows FTIR spectrum of pristine graphite has two peaks at approximately 1668 cm^{-1} due to the skeletal vibration from graphite field (the sp^2 aromatic C=C) and at a 3444cm^{-1} return to the vibration of adsorbed water molecules.

After oxidation process appears O-H stretching vibrations (3100-3405 cm^{-1}), alkoxy stretching vibrations (1040-1170 cm^{-1}), O-H (C-O) distortion peaks (1300-1400 cm^{-1}), the stretching vibration of epoxy (C-O-C) groups (1000-1280 cm^{-1}) and the stretching vibration of carbonyl groups (1700-1730 cm^{-1}). Notably, the aromatic C=C peak could identify them between the scope of 1600-1650 cm^{-1}. In contrast, rGO appears absorption bands are gradually weaker on the reaction path and some of them disappear finally. This evidence the effective removal of oxygen from GO sheets. The spectra of rGO show a little sharp C=C band within the range of (1600-1680 cm^{-1}). Furthermore, It exhibition new band in the region of 2410 cm^{-1} owing to the presence of -CH_2 stretching vibrations[18]. While shows FTIR spectrum of Co_3O_4 nanoparticles including two strong absorption bands at 663.4 and 570.8 cm^{-1}. This proves on the formation the spinel network of Co_3O_4. FTIR analysis A-rGO/Co_3O_4 composite displays strong absorptions band at 663.4 and 570.8 cm^{-1} due to decomposition of the hydroxide to Co_3O_4. Where we note these functional groups are almost removed through the way of thermal treatments, and thus the GO is transformed into rGO. Furthermore, an appearance of absorption bands at 3480, 2889, 1644, 1511 cm^{-1} may be owing to O-H, -CH_2, C=O, C-H of the rGO sheets[19, 20].

Figure (2) the XRD spectra of pure graphite display a sharp peak at 26.5° and weak peak 54.5° that corresponded to d-spacing of (3.36, 1.67)A^o. After oxidation process formation GO a new peaks appears there is a diffraction peaks at 11.6°, 26.5°, 43.9°, which corresponds to an interlayer d-spacing of (7.60, 3.34, 2.12) A^o. While rGO displays the diffraction peaks at 25.7^o, 26.5^o, 27.1^o, which corresponds to an interlayer d-spacing of (3.49, 3.35, 3.28)A^o[19]. Though there is a decrease in the interlayer spacing compared with GO, the basal spacing of rGO is higher than that of single-layer pristine graphene. The higher basal spacing may be due to the presence of residual oxygen functional groups, indicating an incomplete reduction of GO. The XRD spectra of Co_3O_4 nanoparticles display the diffraction peaks (2Θ = 19.09º, 31.35º, 36.92º, 38.62º, 44.87º, 55.71º, 59.42º and 65.30º). This spectrum identical to standard cobalt oxide XRD spectra (PDF Card - Co_3O_4 - 00-042-1467). All diffraction peaks of cobalt oxide can be indicated to cubic spinel Co_3O_4 crystal phase. The very sharp diffraction peaks and high intensity propose the high crystallization of the Co_3O_4 nanoparticles. While the XRD spectrum of A-rGO/Co_3O_4 nanocomposite display diffraction peaks at (2Θ = 19.03º, 31.63º, 36.71º, 38.51º, 45.34º, 56.36º, 59.34º and 65.07º) can be indicated to the cubic spinel Co_3O_4. An additional small broad diffraction peak display at (2Θ = 24.5-29.5°) that can be owing to the irregular accumulate rGO sheets, while the diffraction peak of GO sheet approximately disappeared. The peak positions can be completely indicated to the face-centered cubic[21]. Table (1) shows the diffraction angles, d-spacing values, and the crystalline size of prepared nanomaterials.

Table 1: Values 2Θ, d-spacing and D of prepared nanomaterials

Gr			GO			rGO			Co_3O_4			rGO/Co_3O_4		
2Θ	**d (A°)**	**D (nm)**	**2Θ**	**d (A°)**	**D (nm)**	**2Θ**	**d (A°)**	**D (nm)**	**2Θ**	**d (A°)**	**D (nm)**	**2Θ**	**d (A°)**	**D (nm)**
26.5	3.36	29.50	11.6	7.60	8.13	25.7	3.49	2.11	19.09	4.64	45.75	19.03	4.65	140.27
54.5	1.67	37.35	26.6	3.34	14.5	26.5	3.35	5.33	31.35	2.85	52.60	25.47	3.49	43.42
			42.4	2.12	15.1	27.1	3.28	5.34	36.92	2.43	46.95	29.37	3.03	45.91
									38.62	2.32	47.85	31.63	2.82	48.52
									44.87	2.01	47.27	36.71	2.44	21.16
									55.71	1.64	56.36	38.51	2.33	87.93
									59.42	1.55	46.31	45.34	1.99	47.35
									65.30	1.42	51.09	56.36	1.63	58.86
												59.34	1.55	30.82
												65.07	1.43	35.81

The morphology is identified using SEM and TEM. **Figure (3a)** show SEM analysis of GO nanosheets wavy crimped appearance and the surface are hairy and bristly and the edges of the sheets are foggy[22]. In rGO the nanosheets show fluffy and frizzy texture. Which can be referred to the stacking of individual sheets by various self-assembly methods. This gives the exceptional properties of graphene[23]. While the pure Co_3O_4 nanoparticles appear in a circle shape and comprise of agglomerated amassed circles demonstrate a uniform homogeneity in size, shape and excellent connectivity between the circles[24]. In contrast, SEM analysis of A-rGO/Co_3O_4 nanocomposite display rough surface and Co_3O_4 distributed as bright dots uniformly above the surface of rGO. Can be noted that the Co_3O_4 hierarchical spheres are uniformly decorated upon the surface of the rGO nanosheets[25].

TEM image can be used to identify the morphology of prepared nanoparticles by passing a beam of electrons through the sample to give a picture on a phosphor screen so that it can be different from SEM[26]. TEM image of GO shows transparent, uniform, silk and stable under high-energy electron beam[27]. While TEM analysis of rGO sheet demonstrations a wrinkled paper-like structure. This is due to the chemical bonding of carbon atoms in either a single layer or multi layers[28]. The TEM analysis of Co_3O_4 nanoparticles explain are semi-spherical, porous texture, a uniform distribution and very homogeneous[29]. While the TEM image of A-rGO/Co_3O_4 nanocomposite displays uniform size of spindle-like Co_3O_4 nanoparticles distributed in a homogeneous and dense manner on rGO surface. Where we note the inclusion of Co_3O_4 nanoparticles between the interlayers of the graphene nanosheets. Which makes

the stable composite not decomposes after a strong sonication. This prevents accumulation of the Co_3O_4 nanoparticles through thermal treatment [30, 31]. Shown in **Figure (3b).**

The EDX image shows that the prepared A-rGO/Co_3O_4 composite includes only cobalt, carbon, and oxygen is similar to the chemical composition of the nanocomposite. The appearance of the carbon signal in the spectrum returns to the rGO grid. While EDX image of Co_3O_4 contains only cobalt and oxygen. Shown in **Figure (3c).**

AFM A commonly used a technique to identify the atomic steps of the sample surface. It is used to determine the morphology, number of layers, and thickness of the graphene materials. The AFM analysis of GO shows that the thickness is 60nm, which is due to the hydrophilic property because of containing functional oxygen groups and structure a stable colloidal suspension in water, indicating they have a multilayer structure[32]. In contrast, the mean thickness of rGO up to 15.4 nm due to the elimination of oxygen functionality, this shows that the sheets have a monolayer of rGO[33]. The AFM analysis of the Co_3O_4 nanoparticles displays the spherical shapes are distributed irregularly and heterogeneous. Sometimes Co_3O_4 nanoparticles exhibit form agglomerates of different shape and size. It has found the mean thickness of up to 23.79 nm. While the AFM analysis of the A-rGO/Co_3O_4 nanocomposite shows that Co_3O_4 nanoparticles it appears as different light points in height and deposited on the graphene nanosheets. Where we note that rGO nanosheets assembled in multiple layers to give a crisp look, this results in a difference in the estimated height area. Furthermore, The Co_3O_4 nanoparticles are stable and it acts as a barrier to prevent conglomeration rGO layers. Additionally, the height of the Co_3O_4 particles on the rGO sheets is estimated from line scan profile to be about 69.20 nm[34]. Shown in **Figure (4).**

Table 2: The statistical roughness coefficients of prepared samples

Amplitude Factors	GO	rGO	Co_3O_4	A-rGO/Co_3O_4
R_a (nm)	2.36	1.11	3.16	4.03
R_q	3.56	1.54	4.02	5.94
R_{sk}	-0.61	-0.35	-0.15	-0.39
R_{ku}	1.87	1.98	2.99	2.43
Vertical distance	5.41	2.21	2.76	17.62
Thickness (nm)	60.00	15.48	23.79	69.20

The thermal stability of prepared samples were identified using TGA technique and is exhibited in **Figure (5)**. GO is thermally unstable and start to lose weight during heating. The curve of GO show two level of mass loss, the first level appears approximately 69.7% mass loss in the range of 80-248 ^oC that can be due to the evaporation of adsorbed water from GO surface and the pyrolysis of oxygen functional

groups with release CO and CO_2 gases. The second level happened in the range of 248.3-593.1°C with 19.9 % mass loss due to the groups, additionally to carbon oxidation [35, 36]. After reduction process using L-(+)-ascorbic acid note that all these mass losses become less compared with GO. This refers to the removal most of the epoxide, hydroxyl, and carboxyl functional groups through the reduction process. The significant weight loss was 22.3 % at temperatures almost 140-307.7°C, due to the removal of water molecules and the epoxide, hydroxyl, and carboxyl functional groups. While mass loss up to 38.20% in the range 307.7-595.2°C, due to pyrolysis of the carbon structure of the rGO film. Above-mentioned results propose as prepared rGO possesses higher thermal stability than the GO sheet[37]. TGA analysis of cobalt oxide and A-rGO/Co_3O_4 demonstrates that there is no weight lack until up to the temperature 600°C, This indicates the high thermal stability of prepared nanoparticles[38].

Table 3: Thermo analytical results (TG, DSC) of GO, rGO, Co_3O_4 and A-rGO/Co_3O_4

Compound	TG Range (°C)	DSC(°C)	Mass loss%
GO	80-248	103.3	69.7
	248.3-593.1	201.3	19.9
rGO	140-307.7	93.2	22.3
	307.7-595.2	456.6	38.20
Co_3O_4	——	138.3	——
A-rGO/Co_3O_4	——	147.9	——

3-2. Adsorption Study

3-2-1. Effect of the Weight of A-rGO/Co_3O_4 Nanocomposite

It was observed that adsorption of Rh.B dye increased with increasing surface weight due to increased surface area of adsorption. Weight gain also increases the electrostatic attraction between the dye molecules and the effective locations surface[39]. Shown in **Figure (6a)**

3-2-2. Effect of Adsorption time

The removal of Rhodamine B dye by A-rGO/Co_3O_4 nanocomposite is examined at different time intervals as shown in **Figure (6b)**. That the adsorption dye increases with an increase of time up to 8h. After that time, all active sites of the surface become saturated with dye molecules.

3-2-3. Identify the Type of Isotherm adsorption dye

Figure (6c) demonstration the relationship between the quantities adsorbed versus the residual concentration of the dye. Based on the Giles classification, the adsorption Rhodamine B from L-type of this kind shows that the orientation of the adsorbed molecules on the adsorbent surface is horizontal.

3-2-4. Adsorption Isotherm Models

Langmuir isotherm is linear drawing between C_e/q_e vs. C_e. Depending on the correlation coefficient, this isotherm is not compatible with adsorption of Rhodamine B dye. Freundlich isotherm is linear drawing between $\log C_e$ versus $\log q_e$. Depending on the correlation coefficient, this isotherm is compatible with adsorption of Rhodamine B dye. Finally**,** Tempkin isotherm linear plot between $\ln C_e$ versus q_e. Depending on the correlation coefficient, this isotherm is compatible with adsorption of Rhodamine B dye. Shown in **Figure (7)**.

Table 4: Langmuir, Freundlich and Tempkin isotherm constants for Rh.B dye uptake by rGO/Co_3O_4 nanocomposite

Dye	Langmuir equation			Freundlich eq.			Tempkin eq.		
	K_L	q_m	R^2	K_F	n	R^2	K_T	B	R^2
Rh.B	0.003	434.782	0.414	1.098	0.769	0.979	1.256	0.033	0.911

3-2-5. Effect of Temperature and Thermodynamic Study

The effect of temperature of Rh.B adsorption on the surface nanocomposite at different temperatures (10, 20, 30 and 35 ^oC) was investigated. It is using equation 1 to calculate the amount of adsorbent. The plot of amount of adsorbent (q_e) versus equilibrium concentration (C_e) for the purpose of obtaining isotherm adsorption per degree temperature as shown in **Figure (8a)**, show that the amount of adsorbent increase with increasing temperature due to increases the penetration of the adsorbed species into the surface pores and the production of new effective sites with reduce both the thickness of the outer layer surrounding absorbent material and the mass transfer resistance[40].

Table 5: Thermodynamic parameters of adsorption of Rh.B on nanocomposite surface

Dye	ΔH ($kJ.mol^{-1}$)	ΔG ($kJ.mol^{-1}$)	ΔS ($J.mol^{-1}.K^{-1}$)	Equilibrium Constant (K)
Rh.B	+22.481	-0.459	+78.297	1.207

Thermodynamic parameters of adsorption process were calculated and the results showed in Table (5), which illustrates the adsorption process is "endothermic process" as the temperature increases leading to an increased kinetic energy of the molecules adsorbed on the surface adsorbent leading to release dye species. The results showed the adsorption of the chemical type.

3-2-6. Effect of pH

Several different acidic functions were used 2.0-12.0 to study the effect of pH on adsorption of Rh.B dye on the surface of nanocomposite at 20°C and concentration (100 mg/L). **Figure (8b)** shows that the adsorption capacity increases with the increase of the acidic function of the solution due to the increase in the number of negative charges of active sites on nanocomposite surface. This increases the electrostatic attraction between the Rhodamine B layer and the active sites on the adsorbent surface[41].

3-2-7. Effect of Ionic Strength

Figure (8c) shows the effect of different weight sodium chloride (0.001, 0.01, 0.05, 0.1,0.15 0.2, 0.3 and 0.4 g) upon adsorptive capacity of surface of Rhodamine B dye at 20°C. The increasing of salt concentration causing a decreasing in q_e due to a strong competition between the sodium ions and dye ions in the adsorption on active sites the surface including sodium ions characterize by a smaller size compared with dye ions. So the adsorption of sodium ions is faster than the adsorption of dye ions[42].

3-2-8. Kinetic Study

In this paper, two models were used: pseudo-first order and pseudo-second order to explain the adsorption phenomenon. The pseudo-first order represents the linear plot between $\ln(q_e - q_t)$ versus t. Where we obtain to values k_1 from the slope. **Figure (9a)** for Rhodamine B dye illustration that the adsorption applies to pseudo-first order equation depending on the correlation coefficients listed in the table below. **Figure (9b)** return to pseudo-second order model represents the linear plot between t/q_t versus t . q_e and k_2 can then be determined from the intercept and the slope of the plot. Since the adsorption does not apply to pseudo-second order equation based on the values of correlation coefficients.

Table 6: Adsorption kinetics parameters of adsorption of Rh.B on nanocomposite surface

Dye	Pseudo-first order			Pseudo-second order			
	k_1	q_e	R^2	k_2	q_e	h	R^2
Rh.B	0.005	97.621	0.905	5.076	-36.231	0.066	0.020

Table 7: List of some previous work prepared of rGO/Co_3O_4 nanocomposites

Composite	Synthesis Method	Conditions	Size of NPs (nm)	Applications	Ref.
G/Co_3O_4	Hydrothermal method	GO, $CoCl_2$, NaOH, H_2O_2, $NaBH_4$, 100^{O}C , 2h	31.4	Removal of heavy metal using adsorption process	[13]
Co_3O_4/rGO	Surfactant-assisted method	$CoCl_2$, urea, PVP, GO, hydrazine, 4h,100°C, 2^{step} (600°C, 3h, 300°C, 6 h)	100	Lithium-ion batteries	[43]
GO-Co_3O_4	————	GO, $Co(NO_3)_2$ Hexanol, 140°C, 10h	100	degradation of Orange II in water by advanced oxidation technology	[44]
Co_3O_4/N-rGO	Hydrothermal method	GO, $Co(OAc)_2$, NH_4OH, ethanol, 10 h, 80°C, 2^{step}(150°C, 3h)	12-25	Heterogeneous catalysis	[45]
Co_3O_4/G	Microwave-assisted method.	GO, $Co(NO_3)_2$, urea, microwave oven, 10 min, 2^{step} 320°C, 1h	3-5	Supercapacitors	[46]
Co_3O_4/G	Pulse Microwave-assisted Reduction Methods	GO, $Co(NO_3)_2$, ethylene glycol, microwave oven, 6min	——	Supercapacitors	[47]
Co_3O_4/rGO	Hydrothermal method	GO,$CoCl_2$, urea, 95°C, 8 h, 2^{step} 250°C, 4h	10-30	Supercapacitors	[48]
This work	Hydrothermal method	GO, $CoCl_2$, 1h, NaOH, H_2O_2, 100^{o}C, L-(+)-ascorbic acid, 120 ^{o}C 4h, calcination at 150^{o}C for 5h	21-64	Removal of Rhodamine B dye using adsorption process	——

4- Conclusions

An in situ crystallization method has been developed to synthesize A-rGO/Co_3O_4 nanocomposite material for wastewater application. The prepared composite material depends on regular Co_3O_4 nanoparticles distributed on separated rGO nanosheets. The adsorption experiment of this hybrid has been examined on Rh.B dye through quantitatively adding the nanocomposite into the dye solution and real-time observation the spectral changes of the solutions. It displays that the nanocomposite holds very good adsorption capabilities to the dyes under investigation, which can be gradually modified by adjusting the rGO: Co_3O_4 ratios. It can be expected that the A-rGO/Co_3O_4 nanocomposite is also suitable for many other applications such as fabrication of functional polymer composites, sensors, heterogeneous catalysis, and drug delivery.

Reference

[1] J. Shah, M. R. Jan, A. Haq, Y. Khan, Removal of Rhodamine B from aqueous solutions and wastewater by walnut shells: kinetics, equilibrium and thermodynamics studies, Frontiers of Chem. Sci. Eng. 7(4) (2013) 428-436.

[2] M. M. Ayad, A. Abu El-Nasr, Adsorption of cationic dye (methylene blue) from water using polyaniline nanotubes base, J. Phys. Chem. C. 114(34) (2010) 14377-14383.

[3] Y. C. Wong, Y. S. Szeto, W. H. Cheung, G. McKay, Equilibrium studies for acid dye adsorption onto chitosan, Langmuir 19(19) (2003) 7888-7894.

[4] P. Sivakumar, P. N. Palanisamy, Adsorption studies of basic Red 29 by a non-conventional activated carbon prepared from Euphorbia antiquorum L, Int. J. ChemTech Res. 1(3) (2009) 502-510.

[5] M. Liu, C. Chen, J. Hu, X. Wu, X. W. Liu, Synthesis of magnetite/graphene oxide composite and application for cobalt (II) removal, J. Phys. Chem. C 115(51) (2011) 25234-25240.

[6] W. Fan, W. Gao, C. Zhang, W. W. Tjiu, J. Pan, Tianxi Liu, Hybridization of graphene sheets and carbon-coated Fe_3O_4 nanoparticles as a synergistic adsorbent of organic dye, J. Mater. Chem. 22(48) (2012) 25108-25115.

[7] H. He, C. Gao, General approach to individually dispersed, highly soluble, and conductive graphene nanosheets functionalized by nitrene chemistry, Chem. Mater. 22(17) (2010) 5054-5064.

[8] S. Watcharotone, D. A. Dikin, S. Stankovich, R. Piner, I. Jung, G. H. B. D. G. Evmenenko, S. E. Wu, S. F. Chen, C. P. Liu, S. B. T. Nguyen, R. S. Ruoff, Graphene-silica composite thin films as transparent conductors, Nano lett. 7(7) (2007) 1888-1892.

[9] X. Yang, Y. Wang, X. Huang, Y. Ma, Y. Huang, R. Yang, H. Duan, Y. Chen, Multi-functionalized graphene oxide based anticancer drug-carrier with dual-targeting function and pH-sensitivity, J. Mater. Chem. 21(10) (2011) 3448-3454.

[10] J. T. Robinson, F. K. Perkins, Reduced graphene oxide molecular sensors, Nano lett. 8(10) (2008) 3137-3140.

[11] N. Hu, Z. Yang, Y. Wang, L. Zhang, Y. Wang, X. Huang, H. Wei, L. Wei, Y. Zhang, Ultrafast and sensitive room temperature NH_3 gas sensors based on chemically reduced graphene oxide, Nanotechnol. 25(2) (2013) 025502.

[12] P. Liu, K. Gong, P. Xiao, M. Xiao, Preparation and characterization of poly (vinyl acetate)-intercalated graphite oxide nanocomposite, J. Mater. Chem. 10(4) (2000) 933-935.

[13] E. Yavuz, S. T. glu, H. Sxahan, S. Patat, A graphene/Co_3O_4 nanocomposite as a new adsorbent for solid phase extraction of Pb (II), Cu (II) and Fe (III) ions in various samples, RSC Adv. 3(46) (2013) 24650-24657.

[14] Q. Yuanchun, Z. Yanbao, W. Z. Yuanchun, Preparation of cobalt oxide nanoparticles and cobalt powders by solvothermal process and their characterization, Mater. Chem. Phys. 110(2) (2008) 457-462.

[15] M. Yarestani, A. D. Khalaji, A. Rohani, D. Das, Hydrothermal synthesis of cobalt oxide nanoparticles: Its optical and magnetic properties, J. Sci. 25(4) (2014) 339-343.

[16] J. Gao, F. Liu, Y. Liu, N. Ma, Z. Wang, X. Zhang, Environment-friendly method to produce graphene that employs vitamin C and amino acid, Chem. Mater. 22(7) (2010) 2213-2218.

[17] Y. Leng, W. Guo, S. Su, C. Yi, L. Xing, Removal of antimony(III) from aqueous solution by graphene as an adsorbent, Chem. Eng. J. 211-212 (2012) 406-411.

[18] X. Zhang, K. Li, H. Li, J. Lu, Q. Fu, Y. Chu, Graphene nanosheets synthesis via chemical reduction of graphene oxide using sodium acetate trihydrate solution, Syn. Met. 193 (2014) 132-138.

[19] G. Liu, L. Wang, B. Wang, T. Gao, D. Wang, A reduced graphene oxide modified metallic cobalt composite with superior electrochemical performance for supercapacitors, RSC Adv. 5(78) (2015) 63553-63560.

[20] H. W. Wang, Z. A. Hu, Y. Q. Chang, Y. L. Chen, Z. Y. Zhang, Y. Y. Yang, H. Y. Wu, Preparation of reduced graphene oxide/cobalt oxide composites and their enhanced capacitive behaviors by homogeneous incorporation of reduced graphene oxide sheets in cobalt oxide matrix, Mater. Chem. Phys. 130(1) (2011) 672-679.

[21] Z. S. Wu, W. Ren, L. Wen, L. Gao, J. Zhao, Z. Chen, G. Zhou, F. Li, H. M. Cheng, Graphene anchored with Co_3O_4 nanoparticles as anode of lithium ion batteries with enhanced reversible capacity and cyclic performance, ACS Nano 4(6) (2010) 3187-3194.

[22] H. K. Jeong, Y. P. Lee, R. J. W. E. Lahaye, M. H. Park, K. H. An, I. J. Kim, C. W. Yang, C. Y. Park, R. S. Ruoff, Y. H. Lee, Evidence of graphitic AB stacking order of graphite oxides, J. Am. Chem. Soc. 130(4) (2008)1362-1366.

[23] S. Y. Toh, K. S. Loh, S. K. Kamarudin, W. R. W. Daud, Graphene production via electrochemical reduction of graphene oxide: synthesis and characterisation, Chem. Eng. J. 251 (2014) 422-434.

[24] K. Agilandeswari, A. R. Kum, Synthesis, characterization and optical properties of Co_3O_4 by Precipitation method, Int. J. ChemTech Res. 6(3) (2014) 2089-2092.

[25] S. Bai, L. Du, J. Sun, R. Luo, D. Li, A. Chen, C. C. Liub, Preparation of reduced graphene oxide/Co_3O_4 composites and sensing performance to toluene at low temperature, RSC Adv. 6(65) (2016) 60109-60116.

[26] R. Zan, U. Bangert, , Q. Ramasse, K. S. Novoselov, Metal-Graphene Interaction Studied via Atomic Resolution Scanning, Nano Lett. 11(3) (2011) 1087-1092.

[27] G. Wang, B. Wang, J. Park, J. Yang, X. Shen, J. Yao, Synthesis of enhanced hydrophilic and hydrophobic graphene oxide nanosheets by a solvothermal method, Carbon 47(1) (2009) 68-72.

[28] P. Song, X. Zhang, M. Sun, X. Cui, Y. Lin, Synthesis of graphene nanosheets via oxalic acid-induced chemical reduction of exfoliated graphite oxide, RSC adv. 2(3) (2012) 1168-1173.

[29] T. Ozkaya, A. Baykal, Y. Koseoglu, H. Kavas, Synthesis of Co_3O_4 nanoparticles by oxidation-reduction method and its magnetic characterization, Open Chem. 7(3) (2009) 410-414

[30] Y. Haldorai, J. Y. Kim, A.T. E. Vilian, N. S. Heo, Y. S. Huh, Y. K. Han, An enzyme-free electrochemical sensor based on reduced graphene oxide/Co_3O_4 nanospindle composite for sensitive detection of nitrite, Sen. Actuators B Chem. 227 (2016) 92-99.

[31] Y. Zhao, S. Chen, B. Sun, D. Su, X. Huang, H. Liu, Y. Yan, K. Sun, G. Wang, Graphene-Co_3O_4 nanocomposite as electrocatalyst with high performance for oxygen evolution reaction, Sci. reports 5(2015) 7629.

[32] P. Liu, Y. Huang, L. Wang, A facile synthesis of reduced graphene oxide with Zn powder under acidic condition, Mater. Lett. 91(2013)125-128.

[33] D. R. S. Dey, S. Hajra, R. K. Sahu, C. R. Raj, M. K. Panigrahi, A rapid room temperature chemical route for the synthesis of graphene: metal-mediated reduction of graphene oxide, Chem. Commun. 48(12) (2012) 1787-1789.

[34] B. Wang, Y. Wang, J. Park, H. Ahn, G. Wang, In situ synthesis of Co_3O_4/graphene nanocomposite material for lithium-ion batteries and supercapacitors with high capacity and supercapacitance, J. Alloys Compd. 509(29) (2011) 7778-7783.

[35] P. G. Ren, D. X. Yan, X. Ji, T. Chen, Z. M. Li, Temperature dependence of graphene oxide reduced by hydrazine hydrate, Nanotechnol. 22(5) (2010) 055705.

[36] T. Kuila, S. Bose, P. Khanra, A. K. Mishra, N. H. Kim, J. H. Lee, A green approach for the reduction of graphene oxide by wild carrot root, Carbon 50(3) (2012) 914-921.

[37] S. Some, Y. Kim, Y. Yoon, H. J. Yoo, S. Lee, Y. Park, H. Lee, High-quality reduced graphene oxide by a dual-function chemical reduction and healing process, Sci. reports (2013) 3.

[38] J. Feng, H. C. Zeng, Size-controlled growth of Co_3O_4 nanocubes, Chem. Mater. 15(14) (2003) 2829-2835.

[39] P. Banerjee, P. Das, A. Zaman, P. Das, Application of graphene oxide nanoplatelets for adsorption of Ibuprofen from aqueous solutions: Evaluation of process kinetics and thermodynamics, Pro. Safety and Environ. Protection 101 (2016) 45-53.

[40] B. K. Nandi, A. Goswami, M. K Purkait, Removal of cationic dyes from aqueous solutions by kaolin: kinetic and equilibrium studies, Appl. Clay Sci. 42(3) (2009) 583-590.

[41] H. B. Senturk, D. Ozdes, C. Duran, Biosorption of Rhodamine 6G from aqueous solutions onto almond shell (Prunus dulcis) as a low cost biosorbent Desalination 252(1) (2010) 81-87.

[42] T.G. Chuah, A. Jumasiah, I. Azni, S. Katayon, S. Y. T. Choong, Rice husk as a potentially low-cost biosorbent for heavy metal and dye removal: an overview Desalination 175(3) (2005) 305-316.

[43] L. Pan, H. Zhao, W. Shen, X. Dong, J. Xu, Surfactant-assisted synthesis of a Co_3O_4/reduced graphene oxide composite as a superior anode material for Li-ion batteries, J. Mater. Chem. A 1(24) (2013) 7159-7166.

[44] P. Shi, R. Su, F. Wan, M. Zhu, D. Li, S. Xu, Co_3O_4 nanocrystals on graphene oxide as a synergistic catalyst for degradation of Orange II in water by advanced oxidation technology based on sulfate radicals, Appl. Catalysis B Environ. 123 (2012) 265-272.

[45] Y. Liang, Y. Li, H. Wang, J. Zhou, J. Wang, T. Regier, H. Dai, Co_3O_4 nanocrystals on graphene as a synergistic catalyst for oxygen reduction reaction, Nature mater. 10(10)(2011) 780-786.

[46] J. Yan, T. Wei, W. Qiao, B. Shao, Q. Zhao, L. Zhang, Z. Fan, Rapid microwave-assisted synthesis of graphene nanosheet/Co_3O_4 composite for supercapacitors, Electrochim. Acta 55(23) (2010) 6973-6978.

[47] S. Park, S. Jin Park, S. Kim, Fabrication and capacitance of Co_3O_4-Graphene nanocomposites electrode prepared by pulse microwave-assisted reduction methods, Bull. of Korean Chem. Soc. 33 (2012) 4247.

[48] Z. Song, Y. Zhang, W. Liu, S. Zhang, G. Liu, H. Chen, J. Qiu, Hydrothermal synthesis and electrochemical performance of Co_3O_4/reduced graphene oxide nanosheet composites for supercapacitors, Electrochim. Acta 112 (2013) 120-126.

Figure Captions

Fig. 1. FTIR analysis of Gr, GO, rGO, Co_3O_4 and A-rGO/Co_3O_4

Fig. 2. XRD spectra of Gr, GO, rGO, Co_3O_4 and A-rGO/Co_3O_4

Fig. 3. (a) SEM images, (b) TEM images of GO, rGO, Co_3O_4 and A-rGO/Co_3O_4 (c) EDX images of Co_3O_4 and A-rGO/Co_3O_4

Fig. 4. AFM images of GO, rGO, Co_3O_4 and A-rGO/Co_3O_4

Fig. 5. TGA analysis of GO, rGO, Co_3O_4 and A-rGO/Co_3O_4

Fig. 6. Effect of (a) the weight of nanocomposite, (b) adsorption time, (c) Adsorption isotherm of Rhodamine B dye

Fig. 7. Adsorption Langmuir, Freundlich and Tempkin isotherm
Fig. 8. Effect of (a) Temperature, (b) solution pH, (c) ionic strength
Fig. 9. (a) Pseudo-first order, (b) Pseudo-second order kinetic model

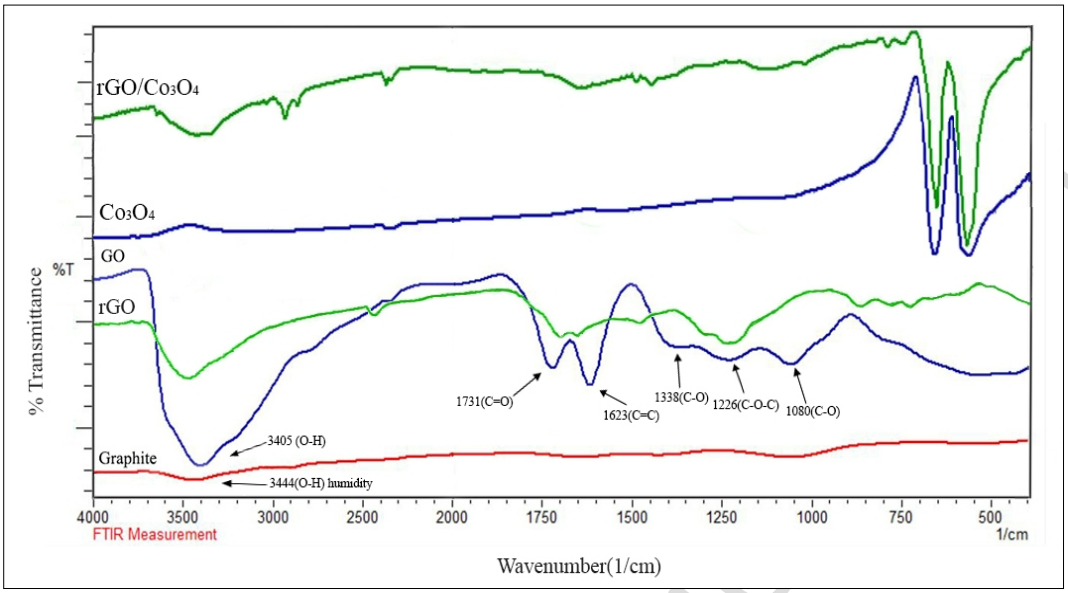

Fig. 1. FTIR analysis of Gr, GO, rGO, Co_3O_4 and A-rGO/Co_3O_4

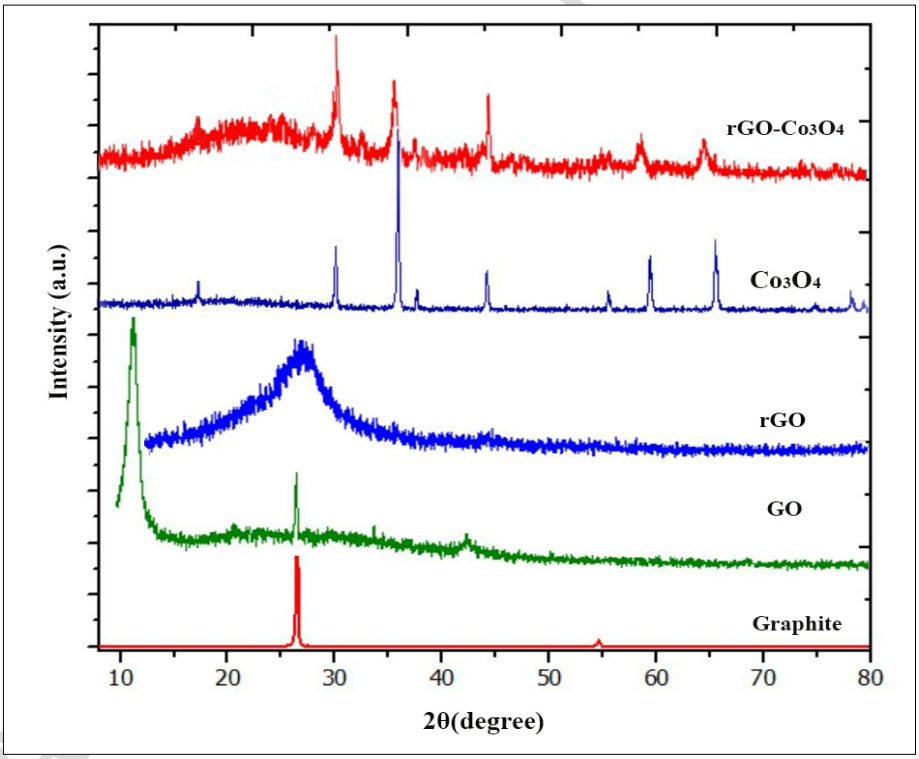

Fig. 2. XRD spectra of Gr, GO, rGO, Co_3O_4 and A-rGO/Co_3O_4

(a)

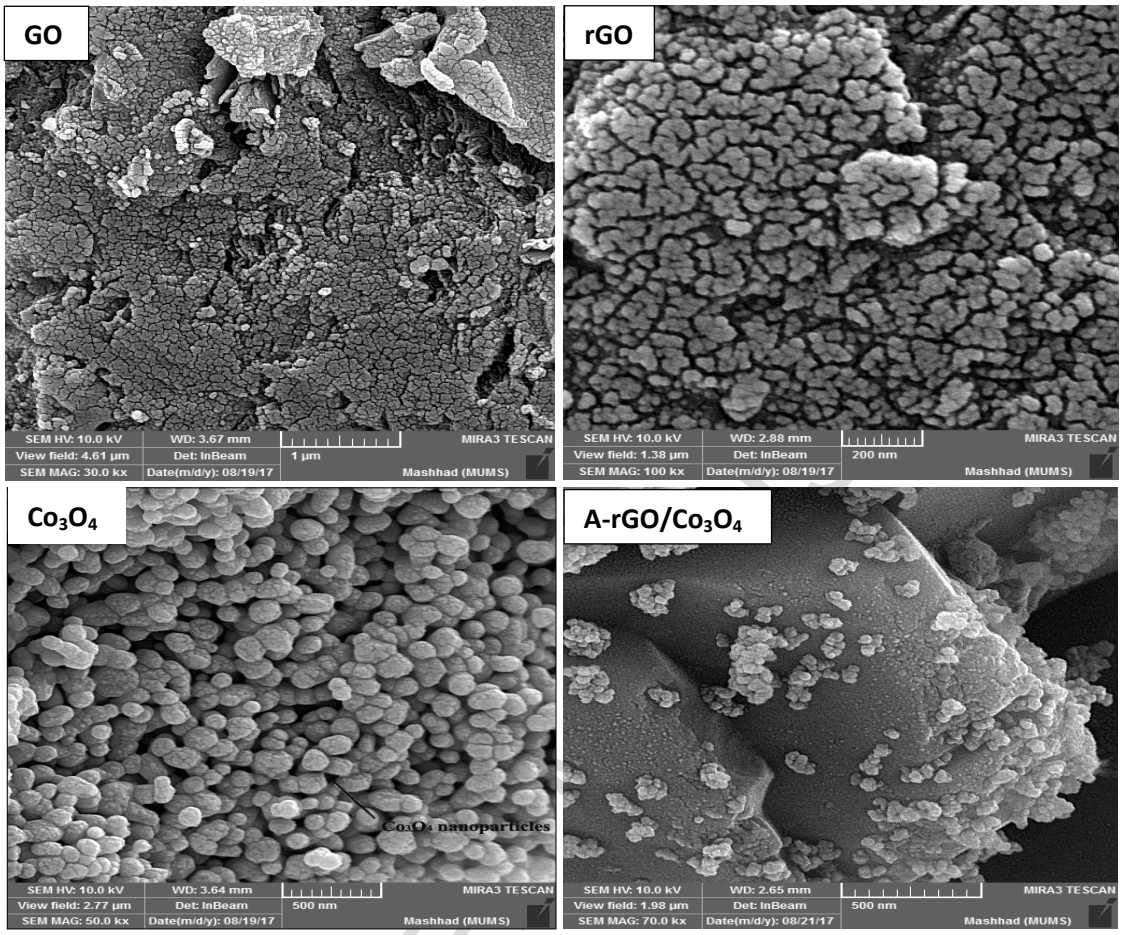
GO
SEM HV: 10.0 kV
WD: 3.67 mm
MIRA3 TESCAN
View field: 4.61 μm
Det: InBeam
1 μm
SEM MAG: 30.0 kx
Date(m/d/y): 08/19/17
Mashhad (MUMS)
rGO
SEM HV: 10.0 kV
WD: 2.88 mm
MIRA3 TESCAN
View field: 1.38 μm
Det: InBeam
200 nm
SEM MAG: 100 kx
Date(m/d/y): 08/19/17
Mashhad (MUMS)
Co3O4
Co3O4 nanoparticles
SEM HV: 10.0 kV
WD: 3.64 mm
MIRA3 TESCAN
View field: 2.77 μm
Det: InBeam
500 nm
SEM MAG: 50.0 kx
Date(m/d/y): 08/19/17
Mashhad (MUMS)
A-rGO/Co3O4
SEM HV: 10.0 kV
WD: 2.65 mm
MIRA3 TESCAN
View field: 1.98 μm
Det: InBeam
500 nm
SEM MAG: 70.0 kx
Date(m/d/y): 08/21/17
Mashhad (MUMS)

(b)

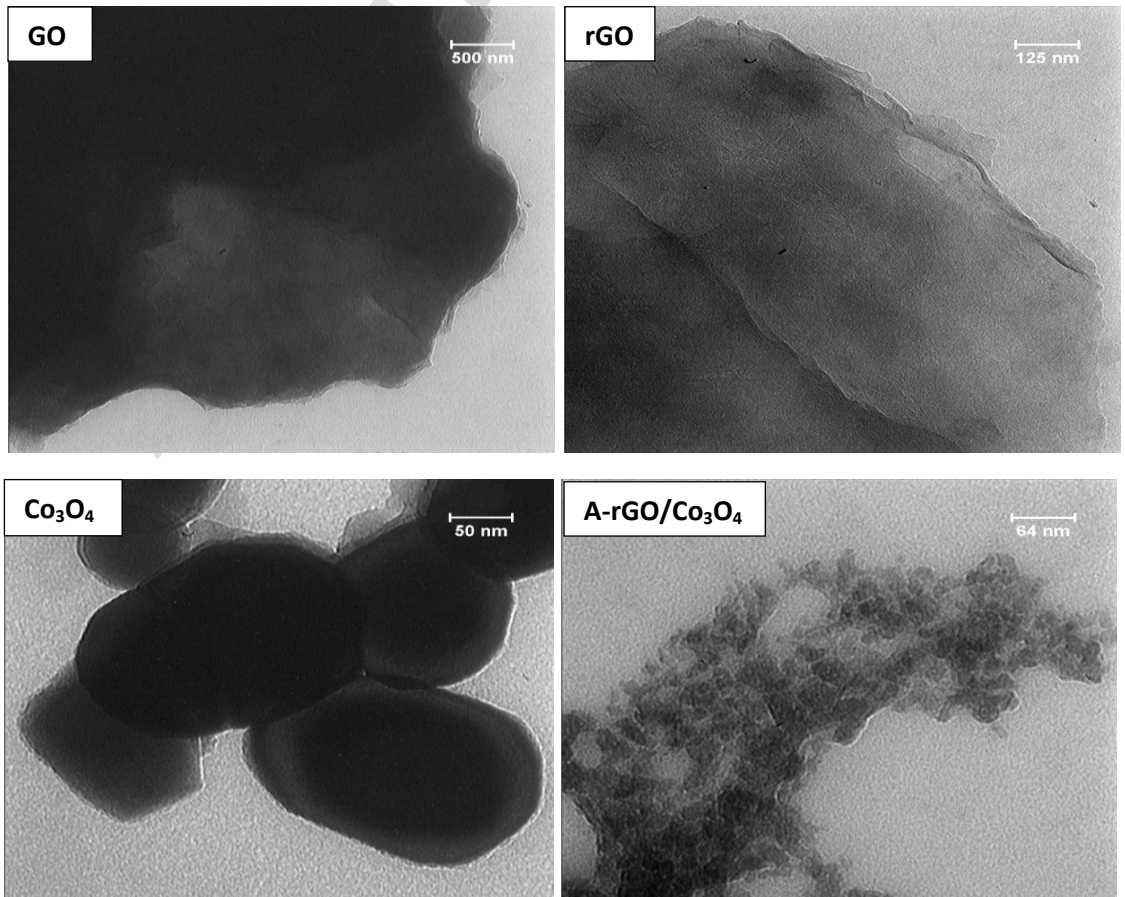
GO
500 nm
rGO
125 nm
Co3O4
50 nm
A-rGO/Co3O4
64 nm

(c)

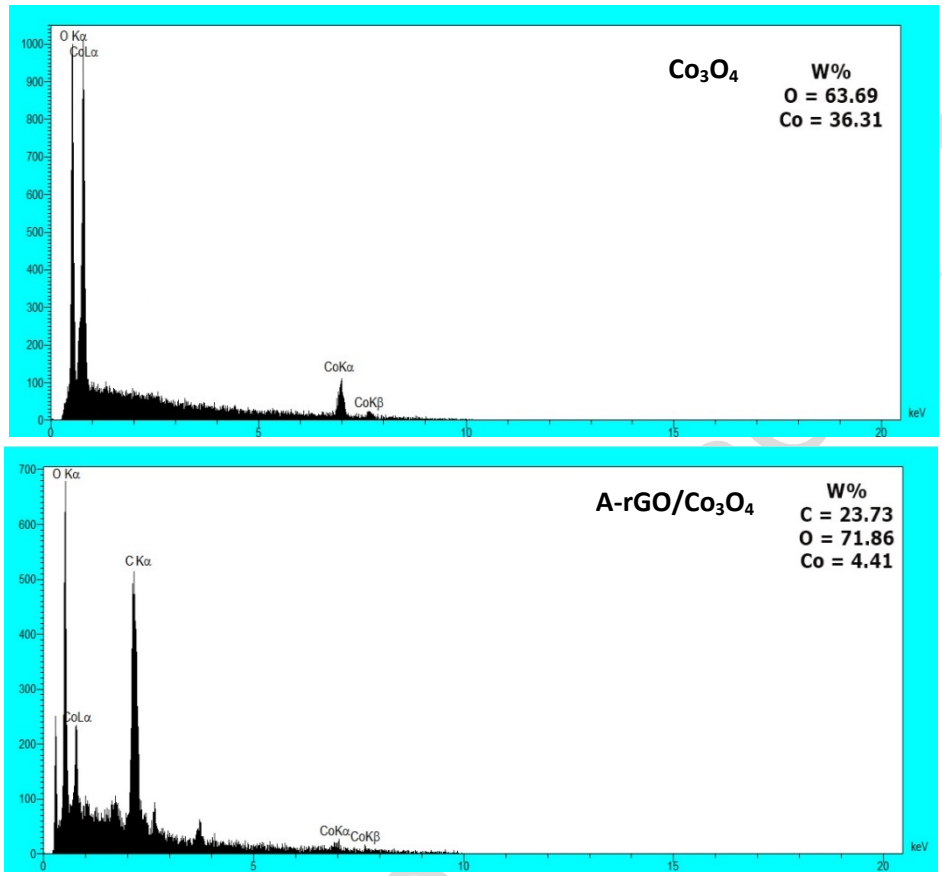

Fig. 3. (a) SEM images, (b) TEM images of GO, rGO, Co_3O_4 and A-rGO/Co_3O_4

(c) EDX images of Co_3O_4 and A-rGO/Co_3O_4

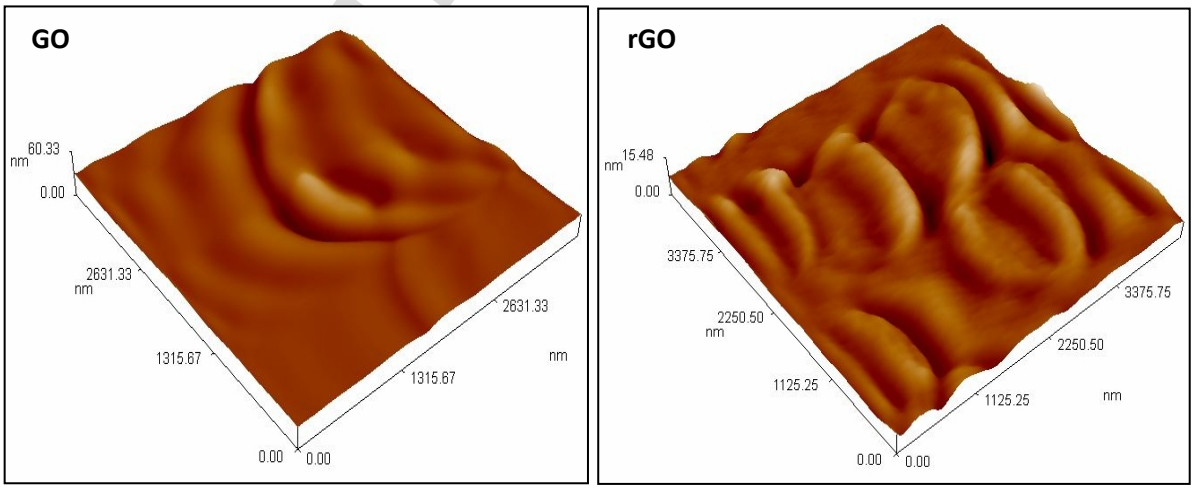

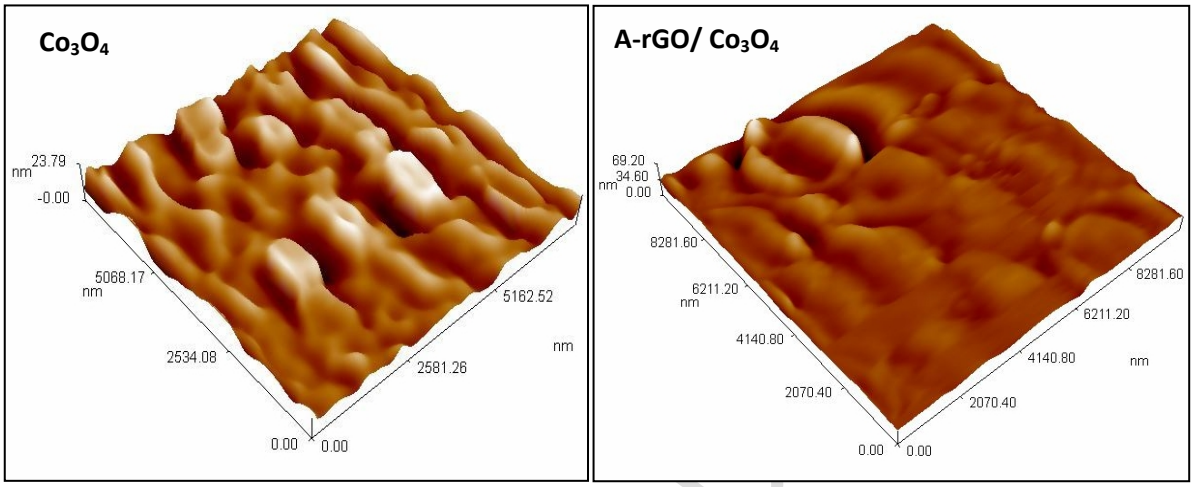

Fig. 4. AFM images of GO, rGO, Co_3O_4 and A-rGO/Co_3O_4

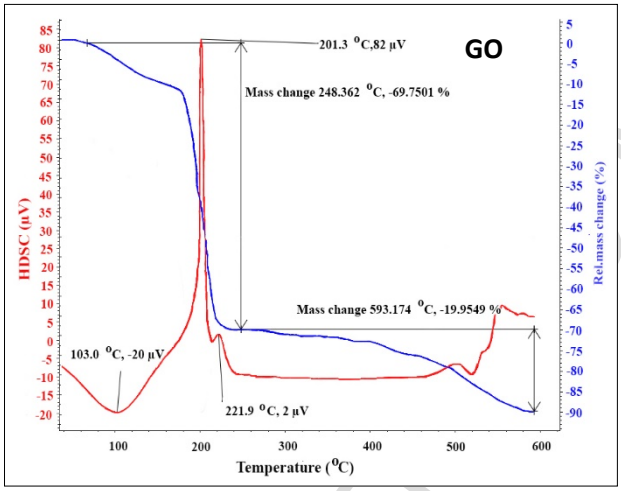

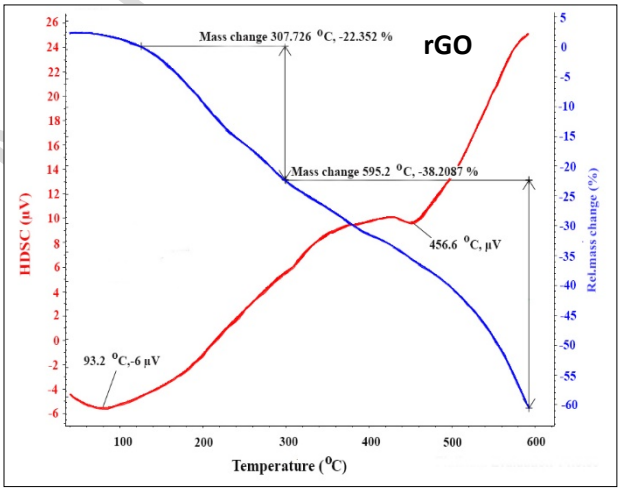

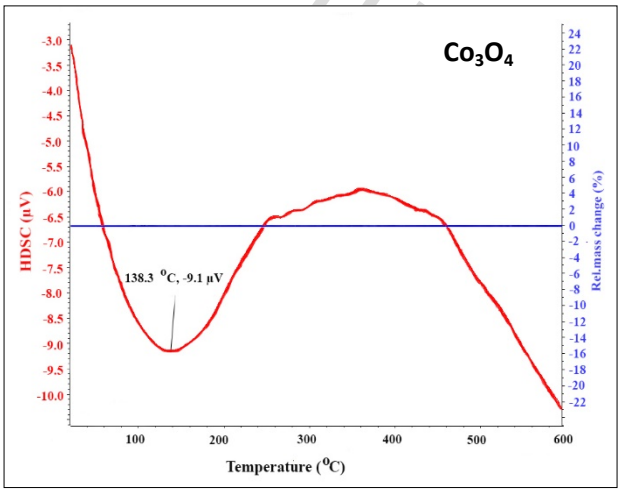

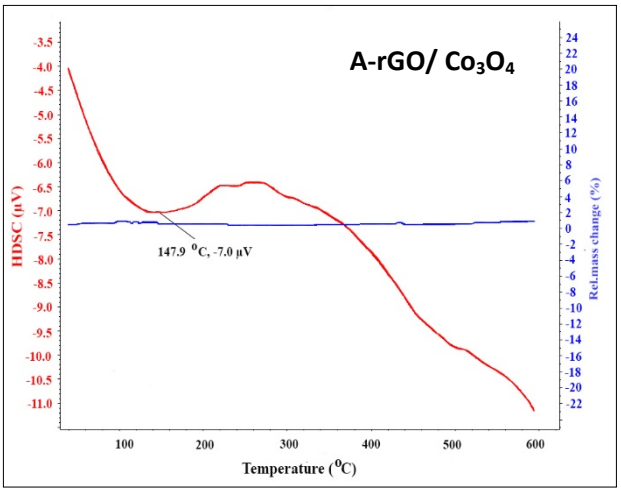

Fig. 5. TGA analysis of GO, rGO, Co_3O_4 and A-rGO/Co_3O_4

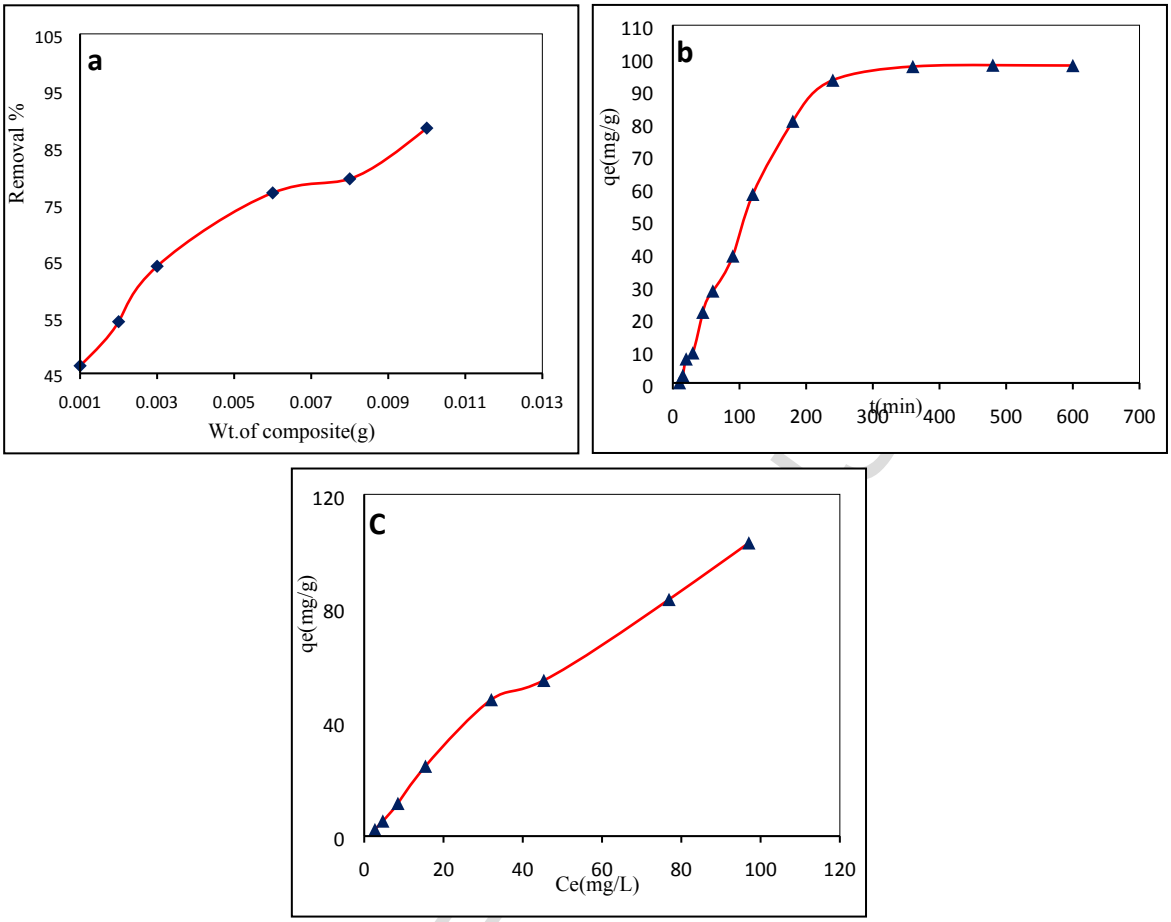

Fig. 6. Effect of (a) the weight of nanocomposite, (b) adsorption time, (c) Adsorption isotherm of Rhodamine B dye

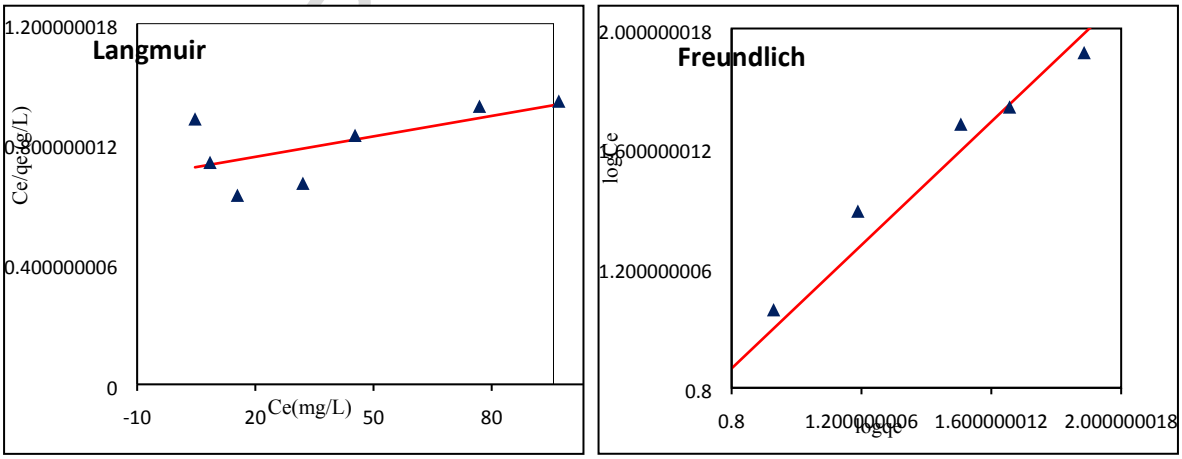

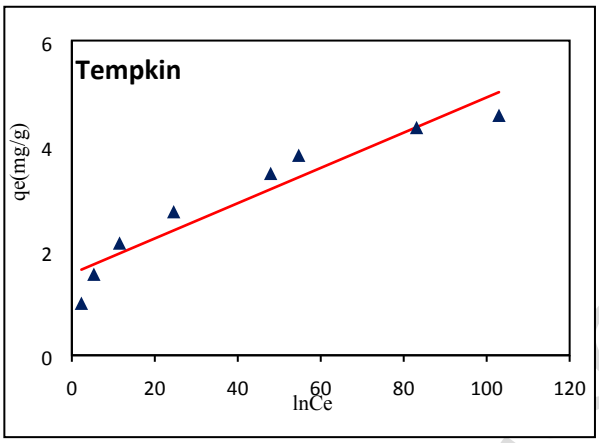

Fig. 7. Adsorption Langmuir, Freundlich and Tempkin isotherm

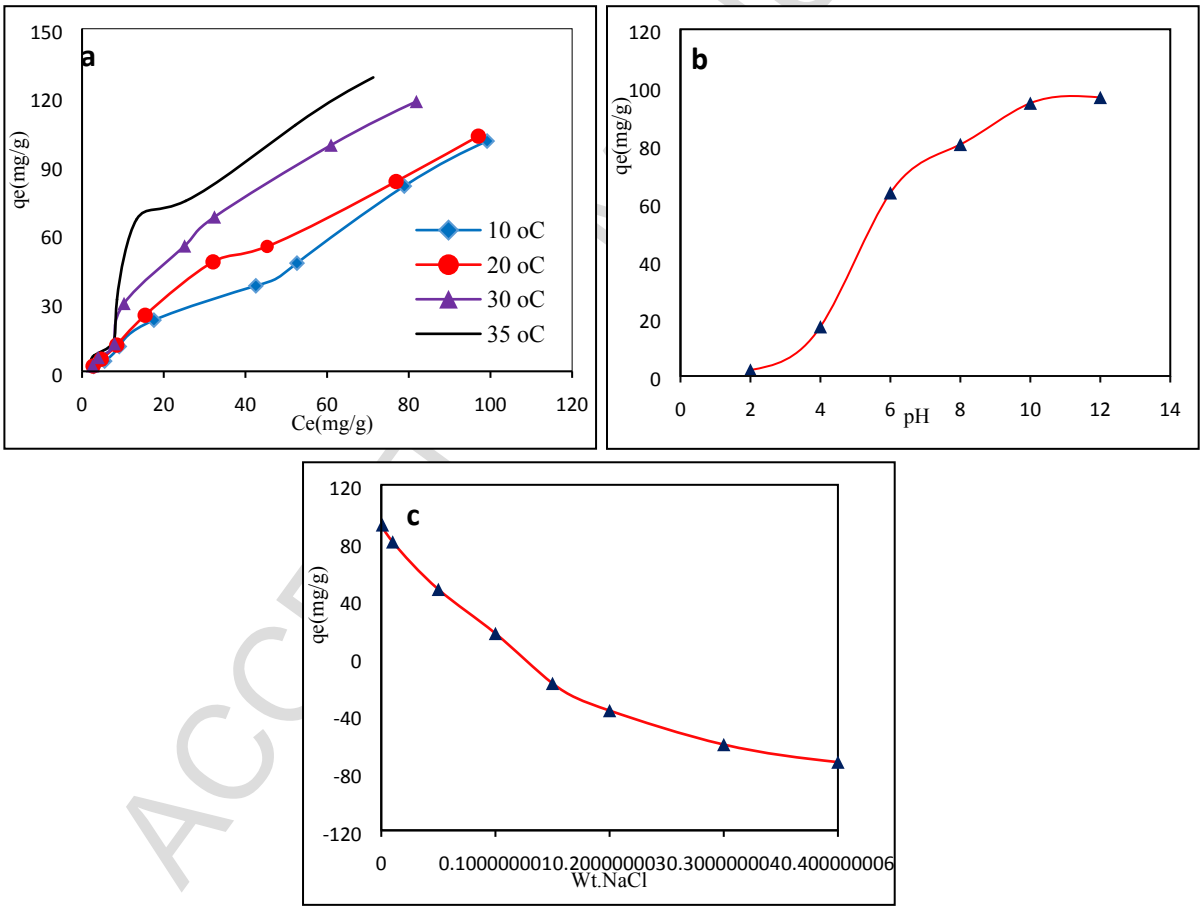

Fig. 8. Effect of (a) Temperature, (b) solution pH, (c) ionic strength

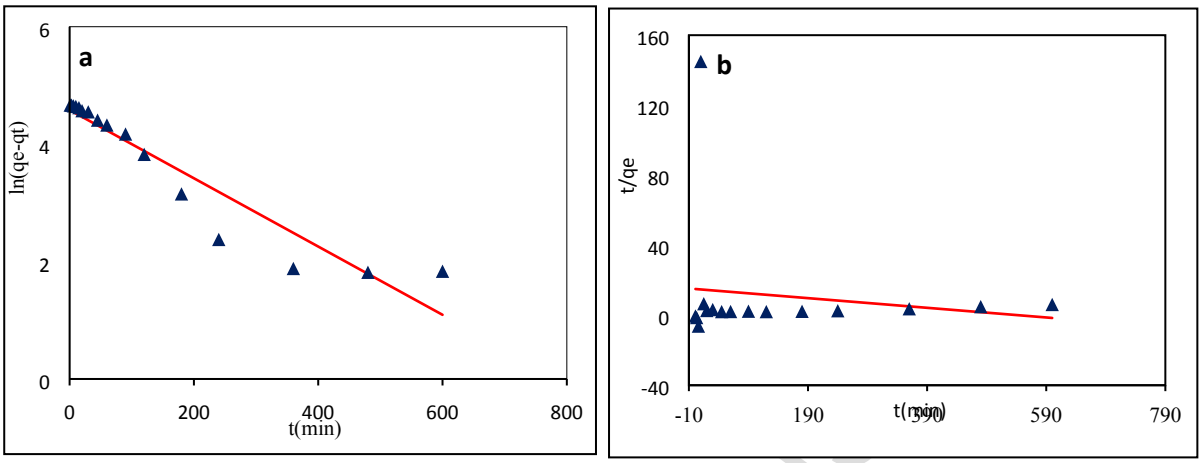

Fig. 9. (a) Pseudo-first order, (b) Pseudo-second order kinetic model